J. Fluid Mech. (2005), *vol.* 533, *pp.* 339–359.
doi:10.1017/S0022112005004362 Printed in the United Kingdom

On the evolution of material lines and vorticity in homogeneous turbulence

By MICHELE GUALA[1], BEAT LÜTHI[1], ALEXANDER LIBERZON[1], ARKADY TSINOBER[2] AND WOLFGANG KINZELBACH[1]

[1]Institute of Hydromechanics and Water Resources Management, Swiss Federal Institute of Technology, ETH Zurich, CH-8093 Zurich, Switzerland

[2]Department of Fluid Mechanics and Heat Transfer, Tel Aviv University, 69978 Tel Aviv, Israel

(Received 27 September 2004 and in revised form 17 January 2005)

The evolution of material lines, l, and vorticity, ω, is investigated experimentally through three-dimensional particle-tracking velocimetry (3D-PTV) in quasi-homogeneous isotropic turbulence at $Re_\lambda = 50$. Through 3D-PTV data the full set of velocity derivatives, $\partial u_i/\partial x_j$, is accessible. This allows us to monitor the evolution of various turbulent quantities along fluid particle trajectories. The main emphasis of the present work is on the physical mechanisms that govern the Lagrangian evolution of l and ω and the essential differences inherent in these two processes. For example, we show that vortex stretching is smaller than material lines stretching, i.e. $\langle \omega_i \omega_j s_{ij}/\omega^2 \rangle < \langle l_i l_j s_{ij}/l^2 \rangle$, and expand on how this issue is closely related to the predominant alignment of ω and the intermediate principal strain eigenvector λ_2 of the rate of strain tensor, s_{ij}. By focusing on Lagrangian quantities we discern whether these alignments are driven and maintained mainly by vorticity or by strain. In this context, the tilting of ω and the rotation of the eigenframe λ_i of the rate of strain tensor s_{ij} are investigated systematically conditioned on different magnitudes of strain, s^2, and enstrophy, ω^2. Further, we infer that viscosity contributes through the term $\nu\omega_i\nabla^2\omega_i$ to $\mathrm{D}\omega^2/\mathrm{D}t$, whereas $\mathrm{D}l^2/\mathrm{D}t$ has no diffusive term. This difference plays a key role in defining the mutual orientation between ω and λ_i. Viscosity thus contributes significantly to the difference in growth rates of $\langle \omega_i \omega_j s_{ij} \rangle$ and $\langle l_i l_j s_{ij} \rangle$.

1. Introduction

One characteristic feature of turbulent flows has been widely recognized as the prevalence of vortex stretching over vortex compression. A commonly held view is that the physical mechanism which leads to $\langle \omega_i \omega_j s_{ij} \rangle > 0$ is the predominant stretching of material line elements. However, it has to be noted that the evolution of vorticity and material elements exhibit qualitative and quantitative differences, some of which are revisited in the present paper with emphasis on the Lagrangian evolution of vorticity and material lines. For a statistically stationary turbulent flow (in Eulerian description) the mean stretching of material lines makes $\langle l^2 \rangle$ grow towards infinity. On the other hand, $\langle \omega^2 \rangle$ remains constant, since the enstrophy production is balanced by its viscous destruction, i.e. $\langle \omega_i \omega_j s_{ij} \rangle = -\langle \nu\omega_i\nabla^2\omega_i \rangle$. The latter equation, integrated over the whole flow field, was also found to be valid at any time (Tsinober 2001). In Lüthi, Tsinober & Kinzelbach (2005) it is inferred that the process of balancing enstrophy production and destruction does not take place locally in space, but

only in a Lagrangian sense, e.g. the terms $\langle \omega_i \omega_j s_{ij} \rangle$ and $\langle \nu \omega_i \nabla^2 \omega_i \rangle$ are balanced if averaged over a few time scales along a particle trajectory. From the representation of the enstrophy production in its terms associated with each eigenvector, λ_i, and eigenvalue, Λ_i, of the rate of strain tensor, s_{ij}, (1.1), it is clear that $\omega_i \omega_j s_{ij}$ is governed not only by the magnitude of ω^2 and Λ_i but also by the mutual orientation between ω and λ_i, as is discussed in Girimaji & Pope (1990), Huang (1996), Ohkitani (2002) and Tsinober (2001),

$$\omega_i \omega_j s_{ij} = \omega^2 \Lambda_1 \cos^2(\lambda_1, \omega) + \omega^2 \Lambda_2 \cos^2(\lambda_2, \omega) + \omega^2 \Lambda_3 \cos^2(\lambda_3, \omega). \tag{1.1}$$

We can therefore expect that the balancing of $\langle \omega_i \omega_j s_{ij} \rangle$ and $\langle \nu \omega_i \nabla^2 \omega_i \rangle$ is reflected also in the Lagrangian evolution of the mutual orientation between ω and λ_i which may be largely influenced by the viscous term $\langle \nu \omega_i \nabla^2 \omega_i \rangle$ (see also Tsinober & Galanti 2003).

To further elucidate the relation between $\langle \omega_i \omega_j s_{ij} \rangle$ and $\langle \nu \omega_i \nabla^2 \omega_i \rangle$, we expand on the important differences between material line stretching and vortex line stretching for which a detailed list of differences is given in Tsinober (2001). By doing this, we are also able to fully appreciate the qualitative differences of the process of enstrophy production as compared to the production of material line energy.

It is emphasized in Tsinober (2001) that the Lagrangian evolution of vorticity differs from the evolution of material lines. It is clear that for each point there exists an infinite number of material elements, but only one single vortex line. Lüthi *et al.* (2005) found clear indication that viscosity plays a significant role in the evolution and dynamics of vorticity. A more qualitative difference is that material lines are passively driven by the field of velocity derivatives, whereas in the case of enstrophy production there exists a complex dynamic coupling between the field of strain and the field of vorticity. For example by comparing the transport equations (1.2), (1.3) and (1.4) for l^2, ω^2 and s^2

$$\frac{1}{2}\frac{\mathrm{D}l^2}{\mathrm{D}t} = l_i l_j s_{ij}, \tag{1.2}$$

$$\frac{1}{2}\frac{\mathrm{D}\omega^2}{\mathrm{D}t} = \omega_i \omega_j s_{ij} + \nu \omega_i \nabla^2 \omega_i, \tag{1.3}$$

$$\frac{1}{2}\frac{\mathrm{D}s^2}{\mathrm{D}t} = -s_{ij} s_{jk} s_{ki} - \tfrac{1}{4} \omega_i \omega_j s_{ij} - s_{ij} \frac{\partial^2 p}{\partial x_i \partial x_j} + \nu s_{ij} \nabla^2 s_{ij}, \tag{1.4}$$

we note that s^2 and ω^2 are not only coupled through the field of velocity, which they both uniquely define, but that this is a two way coupling, whereas it is one way for the material line and the field of velocity derivatives. For example, strong enstrophy production directly reduces the intensity of strain, see (1.4), and therefore strong enstrophy production is directly involved in enstrophy damping.

In the last decade, a number of numerical studies were devoted to the investigation of statistical properties of material lines and vorticity in a turbulent flow field. Stretching rates of material lines, l, and surfaces, $N = l_1 \times l_2$, have been addressed by Drummond & Münch (1990), both in a Gaussian flow field and in a more realistic Gaussian-modified flow, in order to avoid the time-reversal invariant constraint. Girimaji & Pope (1990), Huang (1996) and Kida & Goto (2002) used DNS data to follow the Lagrangian evolution of l and N in isotropic turbulence. Of particular interest in our context is the work of Ohkitani (2002) and Tsinober & Galanti (2003). The preferential orientation of vortex lines and material line elements with respect to the eigenframe of strain is studied by means of DNS. The important

novelty is that for the evolution of material lines a diffusive term is also added, leading to $\mathrm{d}l_i/\mathrm{d}t = l_j \partial u_i/\partial x_j + \nu \nabla^2 l_i$. In this particular case, they find that l tends to align with the intermediate principal strain axis, λ_2, in a Navier–Stokes equation velocity field, whereas in a Gaussian velocity field material lines predominantly align with λ_1.

The first attempt to address these issues experimentally was made by Lüthi *et al.* (2005). This became possible owing to the development of the three-dimensional particle-tracking velocimetry (3D-PTV) experimental technique which allowed for the estimate of the Lagrangian evolution of the full tensor of velocity derivatives with sufficient accuracy (Lüthi *et al.* 2005). The main purpose of the present investigation is to shed more light on the several kinematic and dynamic mechanisms that govern the evolution of material line elements, as compared to the evolution of vorticity. The Lagrangian approach allows us to not only reproduce the statistical properties of ω and l but, more importantly, it allows us to look at the Lagrangian evolution of the quantities of interest. In other words, the presented approach allows us to, e.g. observe – and to some degree understand – the underlying history of ω and l alignments with respect to an evolving eigenframe of strain. Here, our focus lies on quantities which are directly involved in the evolution of vorticity and material lines, i.e. ω^2 and l^2, Λ_i, $\cos(\omega, \lambda_i)$, and $\cos(l, \lambda_i)$. Special attention is given to the dynamic interaction of vorticity with its surrounding flow. In particular, we investigate the influence of ω^2 and s^2 on the rotation Ω_λ^2, of the eigenframe of strain (see Nomura & Post 1998), as well as on the tilting of vorticity itself Ω_ω^2. We will show that both Ω_λ^2 and Ω_ω^2 are directly related to the alignment of vorticity with respect to the eigenframe of strain, e.g. to $\cos(\omega, \lambda_i)$.

In particular, we will observe how the latter alignment evolves along particle trajectories, leading to a persistent (ω, λ_i) or a switch $(\omega, \lambda_i \rightarrow \omega, \lambda_j$, with $i \neq j)$ configuration. The occurrence of these switch events in a Lagrangian frame of reference is not surprising (see Majda 1991; Brachet 1992; Andreotti 1997).

By studying the evolution of special material lines l, which are initially exactly aligned to the vorticity vector, we find that viscosity, which is diffusing both the field of vorticity and the field of strain, plays an important role, and that the different behaviour of ω and l, does not substantially depend on the initial orientation of the latter.

The particular mechanisms of self-amplification and self-moderation of vorticity are singled out by conditioning the evolution of trajectories on the evolution of their $\cos(\omega, \lambda_i)$. Events are defined that represent either persistent alignment to one of the eigenvectors, or, sudden changes of vorticity alignment from one to another eigenvector. We will show how the behaviour of Ω_λ^2 and Ω_ω^2 for different types of events is substantially different. It is thus inferred that Ω_λ^2 and Ω_ω^2 play a key role in the dynamic coupling between fields of strain and enstrophy. This is supported by a comparison with their counterpart for material lines, η_l^2, which lacks both the dynamics and the viscous term involved in vorticity evolution. Hence, the tilting of material lines, η_l^2, exhibits a qualitatively different behaviour.

In § 2, we will provide the description of the experimental set-up and a brief summary on the 3D-PTV technique. In § 3, we will focus on the Lagrangian evolution of $\langle \omega_i \omega_j s_{ij}/\omega^2 \rangle$ and $\langle l_i l_j s_{ij}/l^2 \rangle$ and on their contributors that are associated with each eigenvalue, Λ_i, and eigenvectors λ_i, such as to single out the effect of the initial orientation of l on the quantity $\langle l_i l_j s_{ij}/l^2 \rangle$. In § 4, we will focus on the Lagrangian evolution of the same quantities along one single trajectory, in order to detect which physical mechanisms govern the mutual orientation between ω and λ_i. In § 5, we will

investigate those mechanisms on a statistical basis with a particular attention to the role of viscosity on the persistent alignment between ω and λ_2 and the qualitative differences to their counterparts for the material lines.

2. Experimental set-up and data processing

The data analysed here is taken from experiments performed by Lüthi *et al.* (2005), where an extensive description of the facility is given and the accuracy of the 3D-PTV measuring technique is discussed in detail. The experiment was performed in a glass tank of $120 \times 120 \times 140\,\mathrm{mm}^3$ filled with a saturated aqueous solution of copper sulphate ($CuSO_4$), with a density $\rho = 1050\,\mathrm{kg\,m^{-3}}$, a dynamic viscosity $\mu = 1.2 \times 10^{-6}\,\mathrm{m^2\,s^{-1}}$ and an electrical conductivity of $16.7\,\mathrm{ms\,cm^{-1}}$. A turbulent flow is produced and maintained by Lorentz forces, $f_L = j \times B$, where j is the current density between two opposite walls of the tank, with a wall normal current density field of $70\,\mathrm{A\,m^{-2}}$ provided by a power supply, and B is the magnetic field stemming from 2×2 arrays of cylindrical permanent magnets behind each of the two electrodes. The magnets have a diameter of 42 mm and their intensity is over 1 T. In the proximity of each magnet, the forcing produces a torus-like region with a non-oscillating swirling motion that interacts with the three neighbouring swirls generated by the adjacent magnets. This produces a three-dimensional flow regime which propagates towards the centre of the tank resulting in a turbulent flow with zero mean velocity and velocity fluctuations, u_i, of $O(1)\,\mathrm{cm\,s^{-1}}$. The flow is seeded with neutrally buoyant polystyrene particles with diameter of 40 μm, that are illuminated by a continuous 20 W argon laser. The three-dimensional observation volume has the dimensions of $20 \times 15 \times 15\,\mathrm{mm}^3$ and on average is seeded with 75 particles cm^{-3}. Four synchronized CCD progressive scan monochrome cameras, with 8 bit pixel^{-1} and 640×480 pixels resolution, simultaneously sample the flow field at a rate of 60 Hz over a recording time of 100 s. In terms of the estimated Kolmogorov length scale $\eta = 0.5$ mm and time scale $\tau_n = 0.23$ s, the recorded 6000 frames correspond to $430\tau_n$ with a temporal resolution of 14 frames per τ_n, while the observed volume is equivalent to $40 \times 30 \times 30\eta^3$. A detailed description and validation of the 3D-PTV measuring and processing technique can be found in Lüthi *et al.* (2005) and Willneff & Gruen (2002). Here we give only a brief summary on the basic concepts of 3D-PTV. Three-dimensional particle-tracking velocimetry allows for a direct measurement of fluid particle trajectories, velocities and Lagrangian accelerations in a given observation volume. After each fluid tracer particle is detected in each frame in its image-space, its physical location in the object-space is determined through application of stereoscopic principles. In a second step, particle locations of consequent time steps are linked which, if done properly, results in particle trajectories. The basic feature of the spatial-temporal algorithm developed by Willneff & Gruen (2002) is its capability of improving tracking efficiency by combining both the object-space and image-space information, in order to resolve spatial ambiguities. It must be stressed that a higher tracking efficiency leads to an increased number of long particle trajectories. Long particle trajectories are a crucial prerequisite for the ultimate stage of the processing – the determination of accurate velocity derivatives, $\partial u_i/\partial x_j$, along particle trajectories. $\partial u_i/\partial x_j$ at a given location x_0 is computed by a weighted spatial interpolation procedure that requires accurate velocity information from as many points as possible that are sufficiently close to x_0. The computation of $\partial u_i/\partial x_j$ is validated by checking both the local divergence, $\partial u_i/\partial x_i$, which should vanish owing to incompressibility, and the kinematic relation, $\mathrm{D}u_i/\mathrm{D}t = \partial u_i/\partial t + u_j \partial u_i/\partial x_j$, between Lagrangian acceleration $\mathrm{D}u_i/\mathrm{D}t$, directly obtained from

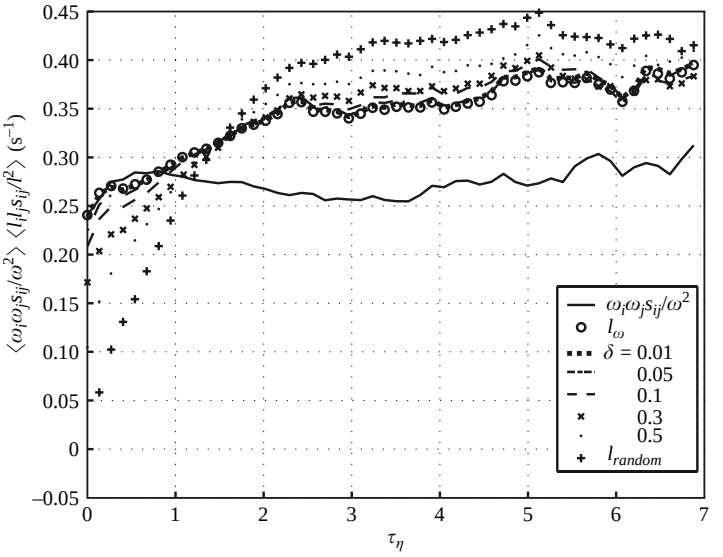

FIGURE 1. Comparison between the mean Lagrangian evolution of the vortex stretching production rate $\langle \omega_i\omega_j s_{ij}/\omega^2 \rangle$ with the stretching rate of the linear elements $\langle l_i l_j s_{ij}/l^2 \rangle$ for different l: those initially exactly aligned with ω (l_ω) and those initially close to ω such that $\cos^2(\omega, l) = 1 - \delta$ for varying δ (l').

particle position, and Eulerian acceleration, $\partial u_i/\partial t$, and convective acceleration, $u_j \partial u_i/\partial x_j$, which both involve the computation of spatial and temporal velocity derivatives.

3. Experimental results on the whole set of trajectories

In this section, we look at the differences of the evolution of different sets of material lines. Special l that are initially perfectly (here and after noted as l_ω), or strongly (denoted as l'), aligned with ω, and random l that have no preferential initial orientation with respect to ω. We demonstrate and explain the different nature of stretching for special and random l. The main outcome of the latter procedure is that the initial orientation has a significant influence on the rate of stretching of material lines, but that it is not sufficient to explain why the vortex stretching rate remain substantially lower than the stretching rate of material elements. Further, having identified the reluctance of special l to give up their predominant alignment with λ_2 before they align with λ_1, we investigate on the tilting of random and special l as well as on the viscous and non-viscous components of vorticity tilting. The latter analysis may shed some light on the contribution to the evolution of vorticity by the viscous term, which is missing in the case of material elements.

3.1. *Special and random l*

Different sets of material lines have been employed in order to compute the mean temporal evolution of $\langle l_i l_j s_{ij}/l^2 \rangle$, as compared to $\langle \omega_i\omega_j s_{ij}/\omega^2 \rangle$, starting from randomly oriented material lines, l, up to material lines with given initial orientation with respect to vorticity, l', such that $\langle \cos^2(\omega, l) \rangle > 1 - \delta$, with $\delta = 0$ (perfect alignment) 0.01, 0.05, 0.1, 0.3, 0.4, 0.5 (see figure 1). The average operator $\langle \cdot \rangle$ is defined as the ensemble average over the spatial domain as a function of the time along each trajectory.

Independently of the precise value of δ, in a range for $0 < \delta < 0.3$, we find that the stretching rate $\langle l'_i l'_j s_{ij}/l'^2 \rangle$ reaches a saturated level that is different from both

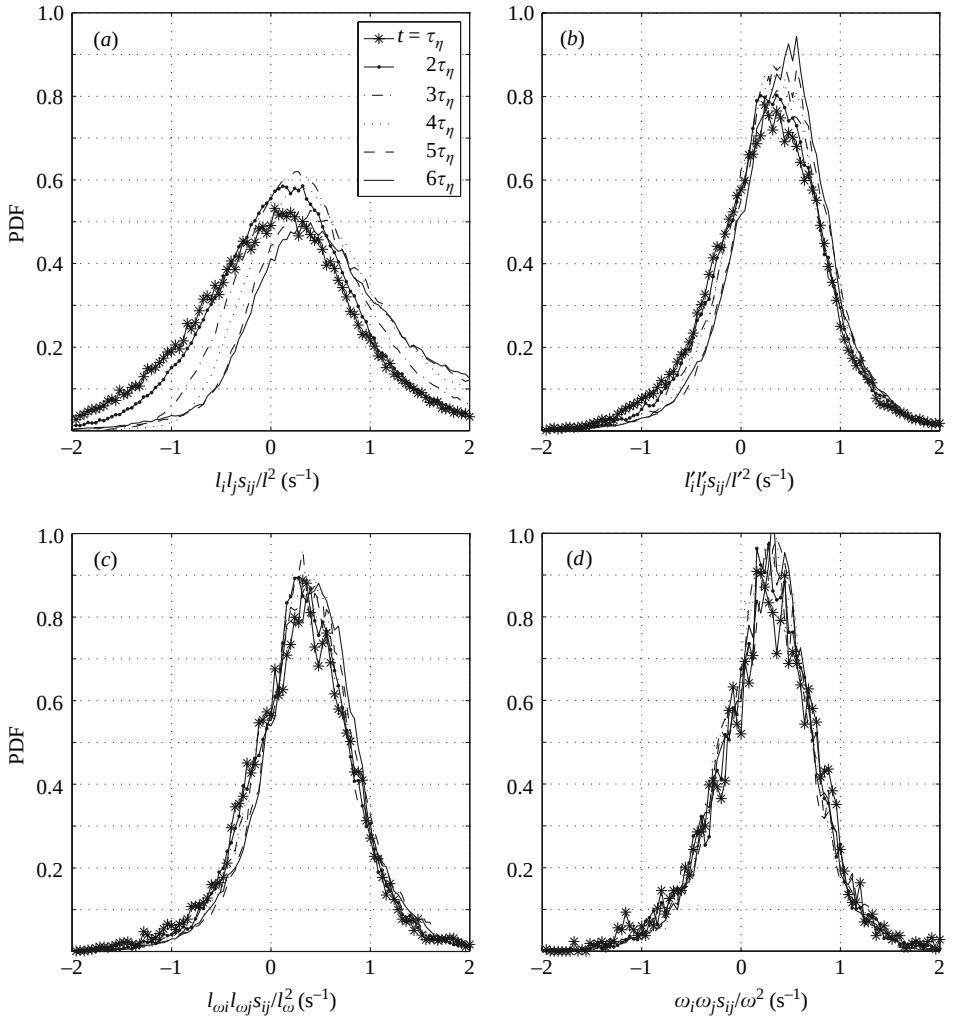

FIGURE 2. Time history of the probability density function of $l_i l_j s_{ij}/l^2$ for (*a*) random l, (*b*) special l' and (*c*) l_ω initially almost perfectly aligned to ω, and (*d*) of $\omega_i \omega_j s_{ij}/\omega^2$.

$\langle l_i l_j s_{ij}/l^2 \rangle$ and $\langle \omega_i \omega_j s_{ij}/\omega^2 \rangle$. This result is used to enlarge the population of special material lines l_ω by including also those l' for the set with $\delta = 0.1$, i.e. $\cos^2(\omega, l(0)) > 0.9$. This allows for a statistical set of l that is large enough to yield convergent results and at the same time is representative of special material lines with perfect initial alignment to vorticity. It is noteworthy that even for l_ω with $\delta = 0$ after an initial period of evolution, we observe a clear difference between the stretching rate $\langle l_{\omega i} l_{\omega j} s_{ij}/l_\omega^2 \rangle$ and the rate $\langle \omega_i \omega_j s_{ij}/\omega^2 \rangle$, the latter being significantly lower.

3.2. *Stretching of special and random l*

The most prominent difference between random l and l_ω lies in their stretching behaviour. Initially, l are stretched much less than l_ω, but already after $\tau_\eta \sim 2$ their stretching rates, $\langle l_i l_j s_{ij}/l^2 \rangle$, are clearly higher than the corresponding rates $\langle l_{\omega i} l_{\omega j} s_{ij}/l_\omega^2 \rangle$ for special material lines (see figures 1 and 2), thus also reflecting a stronger alignment between l and the material line stretching vector $W^l = l_j s_{ij}$ for random l (figure 3). This can be explained when looking at the PDFs of the eigen contributions

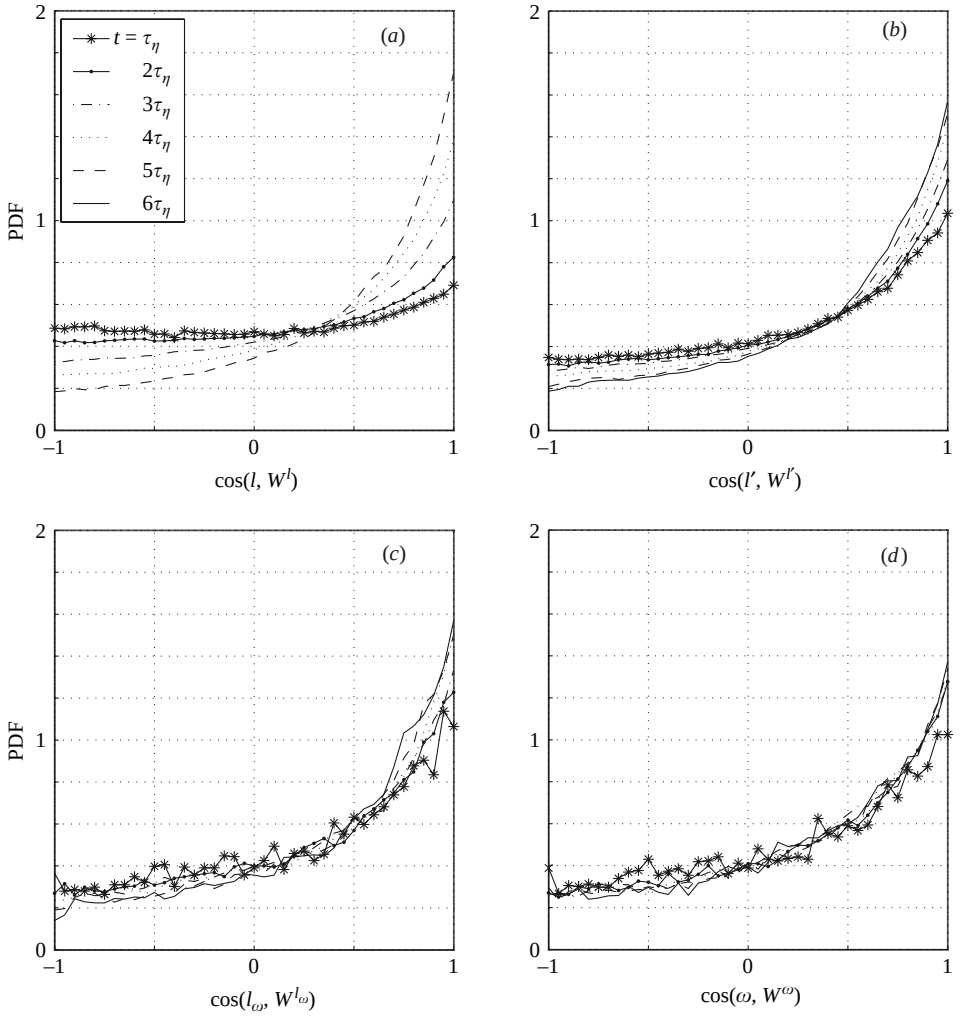

FIGURE 3. Time history of the probability density function of $\cos(l, W^l)$ for (*a*) random l, (*b*) l' initially almost aligned to ω, (*c*) l_ω initially exactly aligned to ω, and (*d*) the probability density function of $\cos(\omega, W^\omega)$.

(expression (3.1)) to $\langle l_i l_j s_{ij}/l^2\rangle$ and $\langle l_{\omega i} l_{\omega j} s_{ij}/l_\omega^2\rangle$ which are shown in figure 4 for different points in time of their evolution

$$l_i l_j s_{ij}/l^2 = \Lambda_1 \cos^2(\lambda_1, l) + \Lambda_2 \cos^2(\lambda_2, l) + \Lambda_3 \cos^2(\lambda_3, l). \tag{3.1}$$

Starting with the initial behaviour at $t \sim 1\tau_\eta$ we see (figure 4) that $l_i l_j s_{ij}/l^2$ has significant contributions from $\Lambda_1 \cos^2(\lambda_1, l)$ and $\Lambda_3 \cos^2(\lambda_3, l)$, which effectively cancel each other, and relatively small contributions from $\Lambda_2 \cos^2(\lambda_2, l)$. This results in an overall small $\langle l_i l_j s_{ij}/l^2\rangle$. On the contrary, for l_ω we know that because of their close ω alignment they are initially predominantly aligned with λ_2, which we know leads to positive stretching rates because $\langle \Lambda_2\rangle > 0$ (see Ashurst *et al.* 1987; Su & Dahn 1996; and Lüthi *et al.* 2005). Consequently, we see in figure 4 only small contributions to $l_{\omega i} l_{\omega j} s_{ij}/l_\omega^2$ stemming from $\Lambda_3 \cos^2(\lambda_3, l)$. At later times, $t \sim 6\tau_\eta$, the situation is different. Random material lines, l, have had enough time to predominantly align with λ_1. This results in stronger contributions from $\Lambda_1 \cos^2(\lambda_1, l)$ and reduced compressing

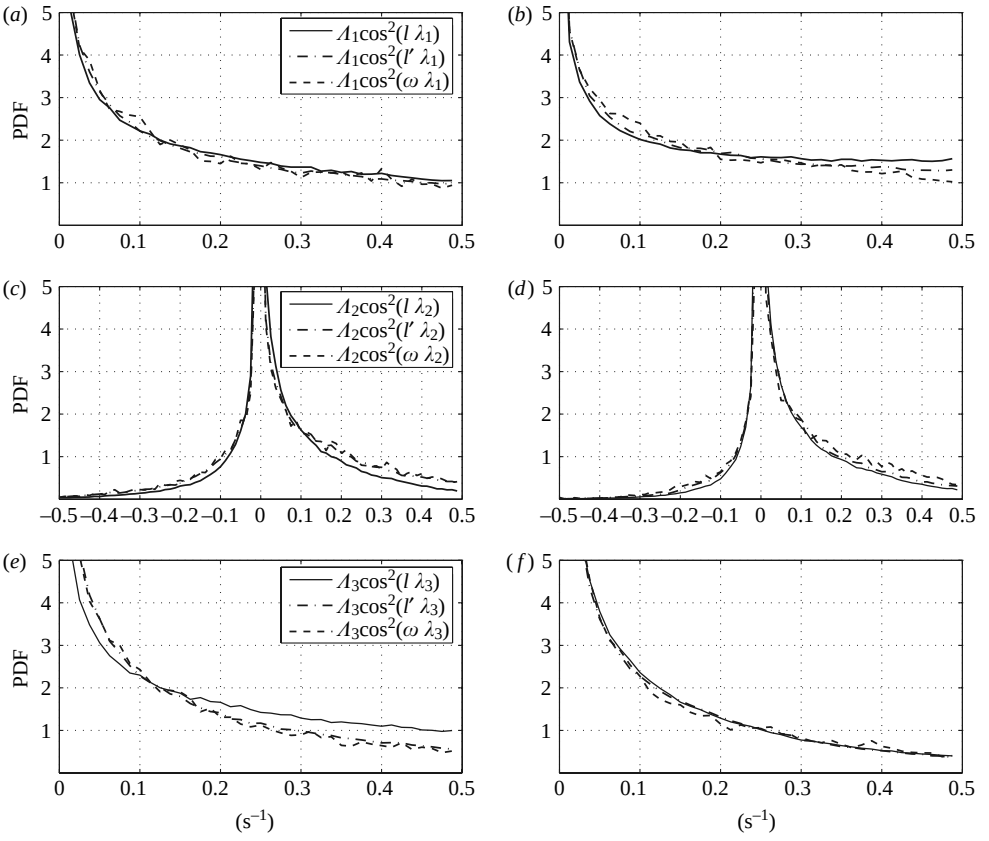

FIGURE 4. Probability density function of $\langle \Lambda_i \cos^2(\lambda_i, \omega)\rangle$ and of $\langle \Lambda_i \cos^2(\lambda_i, l)\rangle$ for random l and for l' initially almost aligned to ω at a initial stage of evolution (a, c, e) and at a mature stage (b, d, f).

contributions from $\Lambda_3 \cos^2(\lambda_3, l)$. The net effect is clear, predominant material line stretching. For l_ω the situation is again different. It was shown by Lüthi *et al.* (2005) that special material lines l_ω are much more reluctant to evolve towards a λ_1 alignment, but that for some time they keep their alignment to ω and consequently also to λ_2. The result is that $\langle l_{\omega i} l_{\omega j} s_{ij}/l_\omega^2\rangle$ remains relatively small also at $t \sim 6\tau_\eta$, because l_ω are still significantly stretched by $\Lambda_2 \cos^2(\lambda_2, l)$, while l, being more aligned with λ_1, experience a stronger contribution by the term $\Lambda_1 \cos^2(\lambda_1, l)$.

3.3. *Tilting of special and random l*

So far we have seen that one important difference in the evolution of vorticity and material line stretching is directly related to their different alignment with respect to the eigenframe, λ_i, i.e. to the cosines of the angle between ω or l and the eigenvectors, λ_i, $\cos(\omega, \lambda_i)$ and $\cos(l, \lambda_i)$. The behaviour of the cosines is the result of the dynamic interaction of the field of vorticity and strain with its surrounding flow. They reflect to what degree the vectors ω or l can follow the changes of direction of λ_i and how much λ_i itself changes its direction. Here, we present the first results with respect to tilting of ω and l and in §§4 and 5, we look also at the changing direction of the eigenframe λ_i. Since its rotation is only accessible if squared owing to the ambiguity in the direction of the eigenvectors λ_i, in the following, we will consistently consider the tilting and the rotation squared.

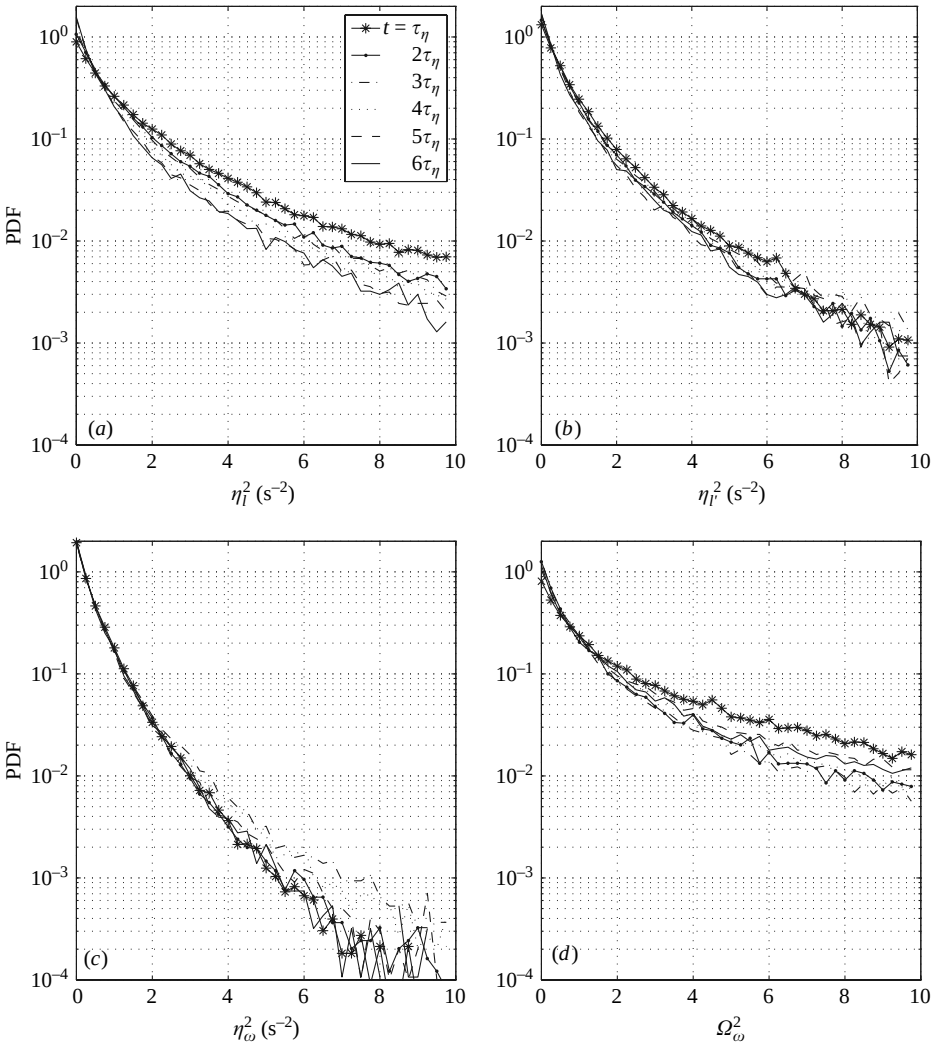

FIGURE 5. Time history of the probability density function of (*a*) the tilting of random l, of (*b*) the tilting of l initially almost aligned to ω, (*c*) of the inviscid tilting of ω, and (*d*) of the true tilting of ω.

The tilting of ω, is defined as $\Omega_\omega^2 = (\mathrm{D}(\omega_i/\omega)/\mathrm{D}t)(\mathrm{D}(\omega_i/\omega)/\mathrm{D}t)$. It is of interest to decompose $\mathrm{D}(\omega_i/\omega)/\mathrm{D}t$ into the sum of an inviscid contribution $\eta_{\omega i}$ and a viscous contribution VT. The former leads to the definition of the inviscid tilting of ω which can be computed as

$$\eta_\omega^2 = \frac{(W^\omega)^2}{\omega^2} - \left\{\frac{\omega_i \omega_j s_{ij}}{\omega^2}\right\}^2. \tag{3.2}$$

Following (3.2), the quantity characterizing the tilting of a material line, η_l^2, is defined as

$$\eta_l^2 = \frac{\mathrm{D}(l_i/l)}{\mathrm{D}t}\frac{\mathrm{D}(l_i/l)}{\mathrm{D}t} = \frac{(W^l)^2}{l^2} - \left\{\frac{l_i l_j s_{ij}}{l^2}\right\}^2 + \frac{l_j s_{ij}(\omega \times l)}{l^2} + \frac{(\omega \times l)^2}{4l^2}. \tag{3.3}$$

In figure 5, the evolution in time of the PDFs for tilting of random and special material line l as well as the total and inviscid tilting of ω are shown. From figure 5,

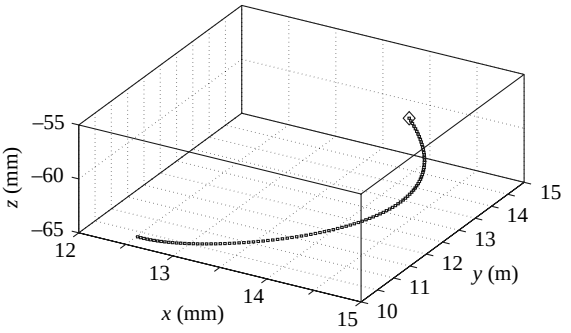

FIGURE 6. Single trajectory plotted in real space; the starting point is indicated with a larger marker.

we observe three main features. First, initially random material lines l tilt more than special material lines l' (figure 5a, b). This is what we can expect from the above results that showed that l change orientation in order to align with λ_1 in a relatively short time, whereas l' are reluctant to give up their λ_2 alignment quickly. Secondly, we see that for l' with $t > 2\tau_\eta$, the PDFs do not change much anymore (figure 5b), as is the case for the inviscid tilting of ω (figure 5c). Thirdly, from figure 5(d), we note that tilting of vorticity is significantly underestimated without taking into account the viscous contribution – it appears that $(\Omega_\omega)^2$ takes considerably larger values than both $(\eta_\omega)^2$ and $(\eta_l)^2$. This can be interpreted as a reflection of the active nature of vorticity as compared to the passive nature of material lines.

4. Experimental results on a single trajectory: the active nature of vorticity

One purpose of studying the evolution of a single trajectory is to demonstrate that vorticity can behave very differently even from special material lines l_ω initially perfectly aligned with vorticity. The selected trajectory, shown in figure 6, is an example where vorticity actively maintains its alignment to λ_2, while an initially identical l_ω has a qualitatively different evolution. Since the situation represents a persistent λ_2 alignment which is actively maintained by vorticity, the selected trajectory can even be looked at as representative of one of the most commonly observed classes in the entire flow. Further, the fact that the trajectory under investigation is dominated by strain rather than by enstrophy is also making the trajectory more representative for the dynamics of the entire flow, since it is strain dominated regions that are dynamically most active, see Tsinober (2001). It has to be stressed, however, that the main reason for investigating the evolution of a single trajectory is to introduce the ideas that will be presented in § 5, where a systematic study of events that represent either persistent alignment of vorticity to one of the eigenvectors, or sudden changes of vortex alignment from one eigenvector to another is performed. In figure 7(a), the evolution of strain, s^2, and enstrophy, ω^2, as well as the evolution of their production terms, $\omega_i\omega_j s_{ij}$ and $s_{ij}s_{jk}s_{ki}$, are shown along the trajectory of figure 6. We note that $\omega_i\omega_j s_{ij}$ takes relatively small values. From figure 7(b), we see that this is the result of $\Lambda_i \cos^2(\omega, \lambda_i)$ contributions to $\omega_i\omega_j s_{ij}$ that balanced each other. From figure 7(c), we see that this balance is achieved mainly through a substantial alignment of ω to λ_2, which is keeping the magnitude of both $\Lambda_1 \cos^2(\omega, \lambda_1)$ and $\Lambda_3 \cos^2(\omega, \lambda_3)$, responsible for strong stretching or compressing, relatively small. Secondly, most of the remaining difference between $\Lambda_1 \cos^2(\omega, \lambda_1)$ and $\Lambda_3 \cos^2(\omega, \lambda_3)$ is compensated by the term

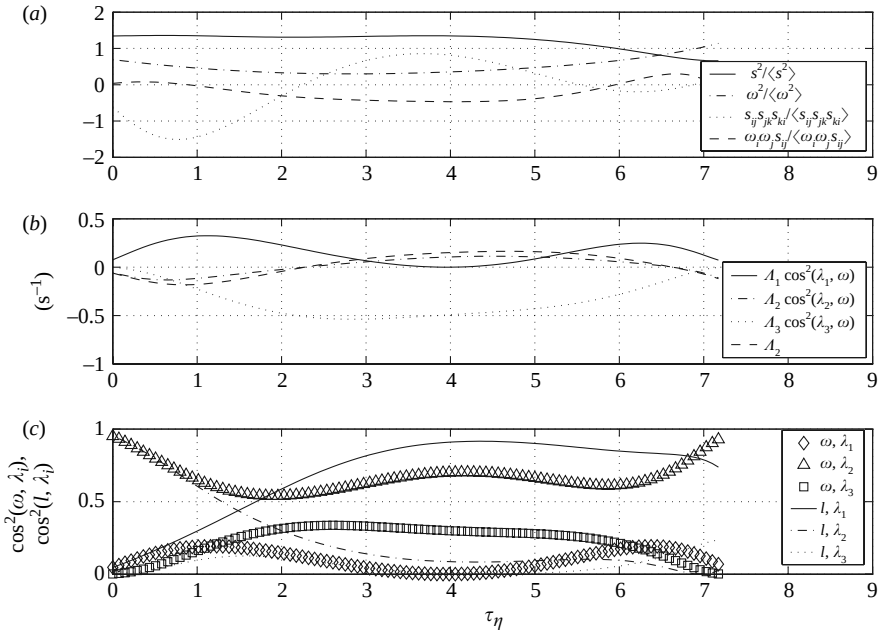

FIGURE 7. Lagrangian evolution along the trajectory of figure 6 of dimensionless strain s^2, enstrophy ω^2, strain production $s_{ij}s_{jk}s_{ki}$ enstrophy production $\omega_i\omega_j s_{ij}$ (*a*), each contribution from the three eigenvalues of the rate of strain λ_i (*b*) and of the alignments between the eigenframe of the rate of strain tensor (λ_i) and ω compared to the alignments between λ_i and the material line l_ω initially parallel to ω (*c*).

$\Lambda_2\cos^2(\omega,\lambda_2)$ which, depending on the sign of Λ_2 can take both negative and positive values. Contrary to the persistent alignment of vorticity to λ_2, we see in figure 7(*c*) that the special material line, l_ω, quickly loses its almost perfect alignment with λ_2 and developes a strong λ_1 alignment. This is an indication that both the viscous term, $\nu\nabla^2\omega$, and the strain–enstrophy interactions, being the main differences between vortex and material line evolution in this situation with identical initial conditions and enviroment, can be responsible for maintaining the $\omega-\lambda_2$ alignment. Both vorticity, ω, and the eigenframe, λ_i, of the rate of strain tensor are participating in maintaining this mutual orientation, as we can see from figure 8 where the evolution of the absolute orientations of ω and of λ_i are monitored along our selected trajectory. During the course of its evolution, two significant events happen. First, at $\tau_\eta\approx 2$, the eigenframe λ_i rotates to find a new and more or less stable position up to $\tau_\eta\approx 6$ (figure 8*a*, *c*). Secondly, at around $\tau_\eta\approx 2$, when $\Lambda_3\cos^2(\omega,\lambda_3)$ reaches a maximum compression contribution to $\omega_i\omega_j s_{ij}$ and when the intermediate eigenvalue Λ_2 changes its sign from negative to positive (figure 7*b*), we see how vorticity also starts to change, or tilt, its direction (figure 8*d*). Subsequently, the alignment of ω and λ_2 is re-established, e.g. the value for $\cos^2(\omega,\lambda_2)$ increases from just above 0.5 to almost 0.7 while the value for $\cos^2(\omega,\lambda_3)$ slowly starts to decrease (figure 7*c*), and consequently, $\omega_i\omega_j s_{ij}$ becomes less compressive. Only by changing its direction does vorticity 'avoid' having the same evolution as the initially identical material line element, l_ω. The net result of these two very different types of behaviour is demonstrated in figure 9(*a*, *b*), which shows that, while the modulus of vorticity changes weakly, the modulus of l_ω continuously increases, driven by its higher stretching rate. We have learned that the persistent

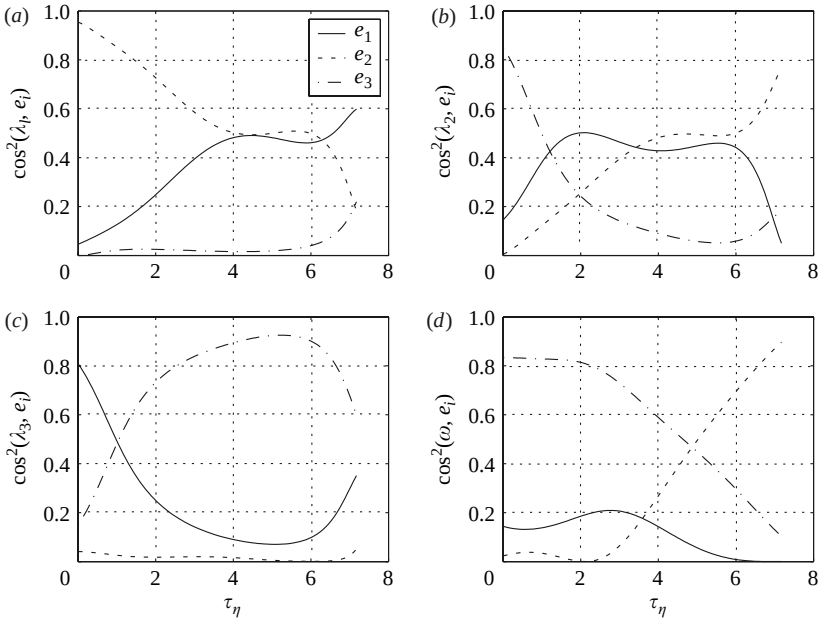

FIGURE 8. Lagrangian evolution of the orientation of the eigenframe of the rate of strain tensor (λ_i) and ω with respect to a fixed reference system e_i.

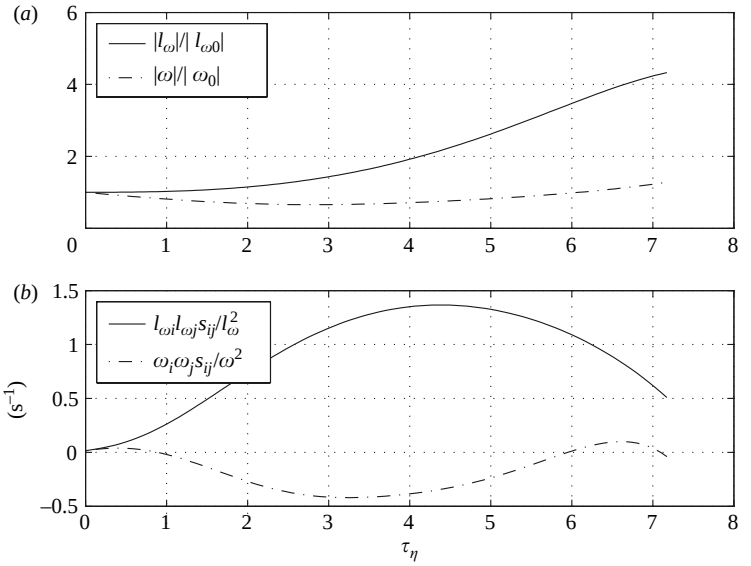

FIGURE 9. Comparison between the Lagrangian evolution of the magnitudes $|l_\omega|$ and $|\omega|$ normalized by the respective values at time $\tau = 0$, and of the rates $\omega_i \omega_j s_{ij}/\omega^2$ and $l_{\omega_i} l_{\omega j} s_{ij}/l_\omega^2$.

alignment of, e.g. ω and λ_2, is the result of the interplay of the rotation of the eigenframe of the rate of strain tensor and vorticity tilting. The mechanisms that govern not only this situation, but also persistent λ_1 and λ_3 alignment of vorticity – hereinafter referred to as 'persistent (ω, λ_i) events', as well as changes of vorticity

orientation from one eigenvector to another, in the following called 'switching (λ_i, λ_j) events' are studied in § 5 in a systematic way on a statistical basis.

5. The combined effect of viscosity and of the active nature of vorticity on the alignment between ω and λ_2

In § 4, we singled out the two mechanisms which govern the mutual behaviour of ω and λ_i, namely the tilting of vorticity and the rotation of the eigenframe λ_i, and we showed how the above-mentioned alignment directly controls a number of quantities, e.g. ω^2, $\omega_i\omega_j s_{ij}/\omega^2$ up to $s_{ij}s_{jk}s_{ki}$. Further, we showed that the behaviour of the alignment between ω and λ_i cannot be interpreted without taking into account both the two-way coupling between the strain and the vorticity fields, and the effect of viscosity in the tilting of vorticity. We provided an indirect estimate of the effect of the viscous term, by observing that the mean inviscid tilting of ω is, in fact, significantly underestimating the mean tilting Ω_ω^2. On the other hand, we showed also how the corresponding alignment between l and λ_i affects the stretching of material lines. In this section, we will study the tilting of vorticity, Ω_ω^2, as well as the rotation of the strain eigenframe Ω_λ^2 on a statistical basis. We will demonstrate how the different behaviour of these quantities can be extracted if they are conditioned on the Lagrangian evolution of the alignment between ω and λ_i, i.e. if they are conditioned on persistent or switching (ω,λ_i) alignment events. This comprises an attempt to elucidate how vorticity and special material lines l_ω initially exactly aligned with vorticity, have a different Lagrangian evolution, and find the role played by the rotation of λ_i, by the tilting of vorticity itself and by the tilting of l_ω, respectively. Persistent and switching events are defined as follows. Each trajectory is divided into different subsets according to the value of $\cos(\omega, \lambda_i)$. We refer to a persistent λ_i alignment event whenever $\cos^2(\omega, \lambda_i)$ stays above the threshold value of 0.7, whereas we refer to a switch $\lambda_i\lambda_j$ event whenever $\cos^2(\omega, \lambda_j) > 0.7$ follows $\cos^2(\omega, \lambda_i) > 0.7$ $(i \neq j)$. An example of a $\lambda_2\lambda_1$ switch on an individual trajectory is shown in figure 10. The threshold value of 0.7, which corresponds to an angle of 33°, is chosen high enough for events to represent strong persistent or switching alignments, and low enough for conditional averages to converge.

For every trajectory subset that is identified either as a switching or a persistent event, the mean value of the following quantities is computed: the tilting of vorticity Ω_ω^2, the rotation of the eigenframe of the rate of strain tensor Ω_λ^2 and the magnitudes of vorticity and strain, ω^2 and s^2. The term Ω_λ^2 is computed by estimating the orientation of the axis of rotation of the eigenframe λ_i and the angle θ spanned by the projection of any eigenvector at time t and $t + \triangle t$ on the plane perpendicular to the axis of rotation. This operation leads to the definition of a unique transformation matrix that operates on $\lambda_i(t = t_i)$ such as to obtain $\lambda_i(t = t_i + \triangle t)$. Eventually $\Omega_\lambda^2 = (\mathrm{D}\theta/\mathrm{D}t)^2$. The above procedure is consistent with the definition proposed by Dresselhaus & Tabor (1991).

The averages Ω_ω^2 and Ω_λ^2 conditioned on both enstrophy and strain magnitude are computed for each trajectory subset, namely for persistent (ω, λ_1), (ω, λ_2) and (ω, λ_3) alignments and also for the switches between (ω, λ_i) and (ω, λ_j) alignments.

5.1. *Results on vorticity*

In the previous section, we inferred that the persistence or the breaking of the alignment between ω and λ_i, could be related to the 'reluctance' of vorticity to

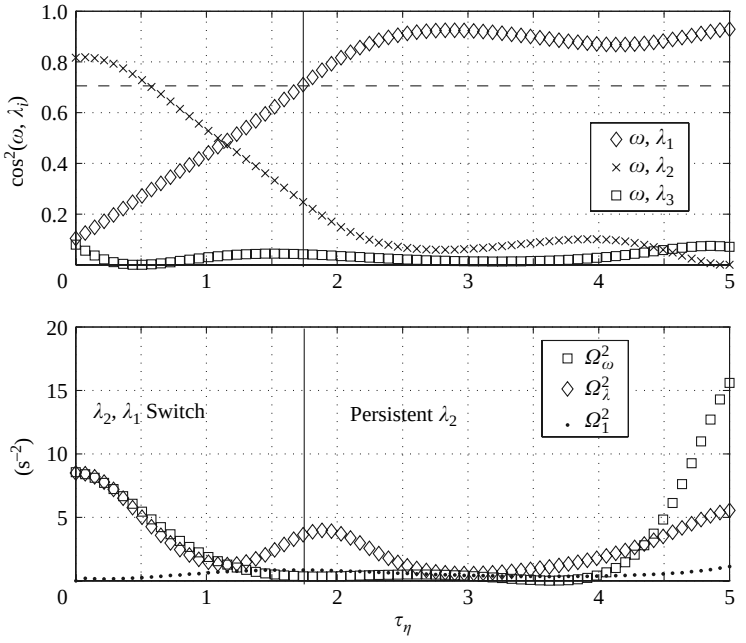

FIGURE 10. $\lambda_2\lambda_1$ switch and persistent λ_2 events in an individual trajectory: Ω^2_ω and Ω^2_λ are computed along the portion of trajectory that is considered active for the $\lambda_2\lambda_1$ switch and are then averaged on the mentioned portion such as to obtain a representative value of $\langle\Omega^2_\omega\rangle$, $\langle\Omega^2_\lambda\rangle$, $\langle\eta^2_\omega\rangle$ for the alignment switch.

Number of persistent alignments	λ_1	λ_2	λ_3
6832	34	53	13

TABLE 1. Number of events characterized by a persistent (ω, λ_i) alignment and their relative percentage contribution.

Number of switch events	$\lambda_1\lambda_2$	$\lambda_2\lambda_1$	$\lambda_3\lambda_2$	$\lambda_2\lambda_3$	$\lambda_3\lambda_1$	$\lambda_1\lambda_3$
6064	28	28	12	15	9	8

TABLE 2. Number of events characterized by a switch of the (ω, λ_i) alignment and their relative percentage contribution.

be too stressed or compressed. Moreover, we showed that vorticity (as well as the eigenframe λ_i) is able to change its orientation, in order, for instance, to maintain the λ_2 alignment. The tendency of vorticity, or of the eigenframe λ_i, to change orientation in the presence of significant strain, or enstrophy, may provide an experimental validation of the latter statements on a statistical basis.

In table 1, the total number of events identified as a persistent alignment is reported along with the percentage contribution of each (ω, λ_1), (ω, λ_2) and (ω, λ_3) alignment. The predominance of the vorticity alignment with λ_2 is clearly seen. The same procedure was carried out for switching events (see table 2). The frequent occurrence of switches between λ_1 and λ_2 supports the idea that vorticity is mostly lying in the plane spanned by λ_1 and λ_2, contributing to positive $\langle\omega_i\omega_j s_{ij}/\omega^2\rangle$. The previously

Conditioned on	$\lambda_1\lambda_2$	$\lambda_2\lambda_1$	$\lambda_3\lambda_2$	$\lambda_2\lambda_3$	$\lambda_3\lambda_1$	$\lambda_1\lambda_3$	λ_1	λ_2	λ_3
s^2	$\omega \sim \lambda$	$\omega \sim \lambda$	ω	$\omega \sim \lambda$	ω	ω	λ	λ	ω
ω^2	λ	λ	λ	λ	λ	λ	λ	λ	λ

TABLE 3. Predominant tilting contribution in the case of switch of $(\omega, \lambda_i)(\omega, \lambda_j)$ alignment (left) and persistent (ω, λ_i) (right).

Number of persistent alignments	λ_1	λ_2	λ_3
$l//\lambda_1$ 5982	79	17	3
$l//\lambda_2$ 6756	17	76	6
$l//\lambda_3$ 8575	14	9	75
$l//\omega$ 5023	35	52	11

TABLE 4. Number of events characterized by a persistent (l, λ_i) alignment and their relative percentage contribution.

Number of switch events	$\lambda_1\lambda_2$	$\lambda_2\lambda_1$	$\lambda_3\lambda_2$	$\lambda_2\lambda_3$	$\lambda_3\lambda_1$	$\lambda_1\lambda_3$
$l//\lambda_1$ 3179	66	11	4	4	2	14
$l//\lambda_2$ 3179	10	66	2	16	2	1
$l//\lambda_3$ 6835	4	6	28	14	57	12
$l//\omega$ 3105	30	39	8	10	7	3

TABLE 5. Number of events characterized by a switch of the (l, λ_i) alignment and their relative percentage contribution.

	λ_1	λ_2	λ_3	$\lambda_1\lambda_2$	$\lambda_2\lambda_1$	$\lambda_3\lambda_2$	$\lambda_2\lambda_3$	$\lambda_3\lambda_1$	$\lambda_1\lambda_3$
$l//\lambda_1$	51	11	2	23	3	1	1	1	4
$l//\lambda_2$	10	46	3	4	26	1	6	1	1
$l//\lambda_3$	7	5	42	2	3	12	1	25	1
$l//\omega$	22	33	7	11	14	3	4	1	2
ω	18	28	7	13	13	6	7	4	3

TABLE 6. Overall percentage distribution of events among persistent and switching alignment for vorticity and different sets of values of l.

estimated experimental error (Lüthi *et al.* 2005) results in an error of approximately $\pm 7^\circ$ in the mutual orientations of ω and λ_i. In order to test how this error affects the results presented in tables 1–6, we proceeded in two ways: (i) we computed the percentage contributions with thresholds values for $\cos^2(\omega, \lambda_i)$ of 0.6 and 0.8, and (ii) we divided the whole set into ten subsets and estimated the standard deviation of the relative contributions for the case of the 0.7 threshold. These two methods, for the ω, λ_i alignments, concur in estimating an absolute error ranging from $\pm 1\,\%$ to $\pm 5\,\%$ depending on the specific percentage contribution. The relative error, defined as the absolute error divided by the correspondent contribution value, is always below $10\,\%$. Since vorticity was shown (e.g. figure 5) to be significantly more active than material lines in terms of tilting, we believe that the latter estimates can be safely extended to the tables addressing the behaviour of material lines.

The mean tilting of vorticity Ω^2_ω and the mean rotation of the eigenframe of the rate of strain tensor Ω^2_λ conditioned on the three persistent (ω, λ_i) events are shown in figure 11.

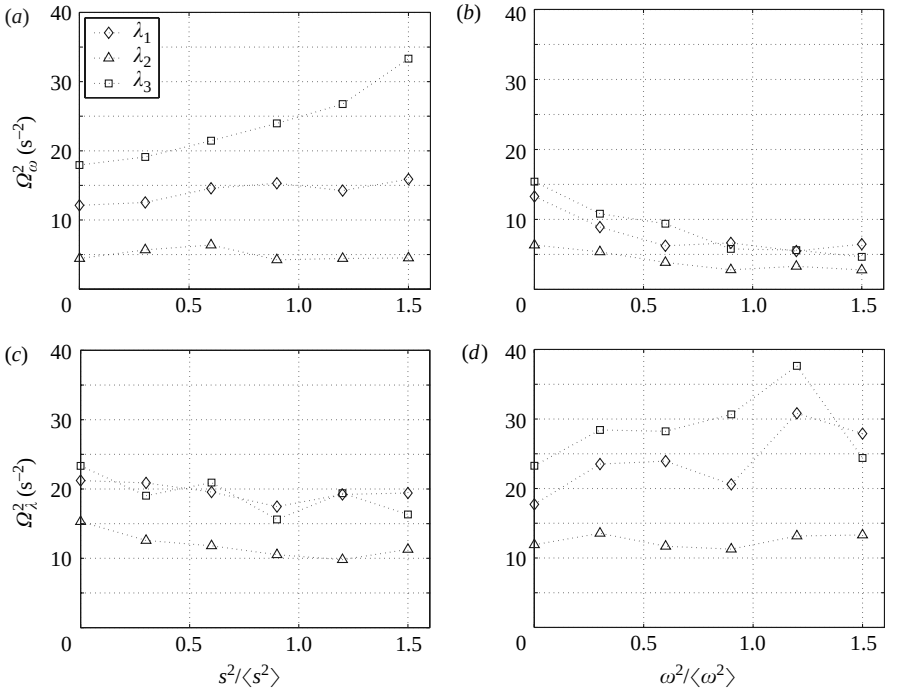

FIGURE 11. Mean contributions of (a, b) the tilting of vorticity Ω^2_ω and (c, d) of the rotation of the rate of the strain eigenframe Ω^2_λ in a condition of persistent (ω, λ_i) alignment conditioned on strain (left) or enstrophy (right).

First, we note that when vorticity is persistently aligned with λ_2, both Ω^2_ω and Ω^2_λ are significantly lower as opposed to the cases of persistent λ_1 and mainly λ_3 alignment, regardless of strain and enstrophy magnitude.

In the case of λ_1 and mainly λ_3 alignment, vorticity is significantly more active in tilting itself, especially when strain is high. This may explain in part why vorticity is statistically aligned to λ_2. The tendency of vorticity tilting and of the eigenframe rotation to evade persistent (ω, λ_1) and (ω, λ_3) suggests that we should expand our investigations also to the switching events. Conditional averages of both Ω^2_ω and Ω^2_λ are thus presented in figure 12 for the complete set of (ω, λ_i), (ω, λ_j) switches.

A qualitative summary of figure 12 is given in table 3, where the dominant mechanism, i.e. either Ω^2_ω or Ω^2_λ, is indicated for all possible configurations, in terms of both persistent and switching events, and strain and enstrophy magnitude.

The main trends are summarized as follows.

As s^2 increases, Ω^2_ω increases, while Ω^2_λ remains practically unaffected The most significant contributions of Ω^2_ω occur when ω is aligned with λ_3, the lowest one, when ω is aligned with λ_2. As expected, vorticity on average changes its orientation in high strain regions reacting to significant stretching and mainly to significant compression (figure 11).

As ω^2 increases, Ω^2_ω decreases while Ω^2_λ slightly increases: the direction of vorticity becomes more and more persistent as its magnitude becomes significant (figure 11).

The above trends are observed for both persistent and switch events (see figure 12). In particular whenever the (ω, λ_3) alignment is involved in high strain regions, the tilting of vorticity is dominant.

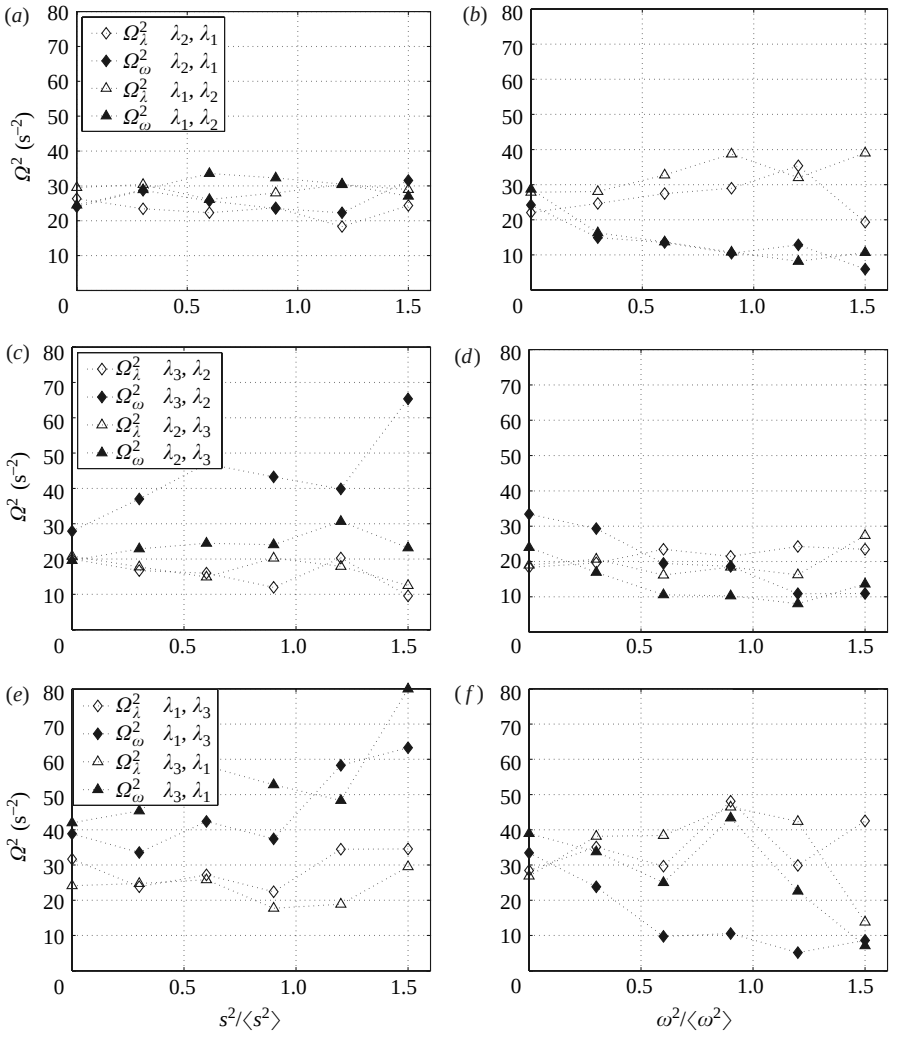

FIGURE 12. Mean contributions of the tilting of vorticity Ω^2_ω and of the rotation of the rate of the strain eigenframe Ω^2_λ during the switches (ω, λ_i)–(ω, λ_j) alignments conditioned on strain (left) or enstrophy (right).

5.2. *Results on material lines*

In the framework of the comparative analysis between ω and l, an analogous procedure has been carried out focusing on the persistent and switching events governed by the alignment between l and λ_i. Again, each trajectory is divided into different subsets according to the value of cos(l, λ_i). We define a persistent λ_i event whenever $\cos(l, \lambda_i)$ stays above the threshold value of 0.7 and a switching (λ_i, λ_j) event whenever $\cos(l, \lambda_j) > 0.7$ follows $\cos(l, \lambda_i) > 0.7$ $(i \neq j)$, in complete analogy with the treatment of vorticity. This analysis has been performed for four different initial conditions for l, namely, $l \| \lambda_1$ initially exactly aligned with λ_1, $l \| \lambda_2$ initially exactly aligned with λ_2, $l \| \lambda_3$ initially exactly aligned with λ_3, $l \| \omega$ initially exactly aligned with ω.

The statistics on the occurrence of persistent and switching events is summarized in tables 4 and 5, respectively. The overall behaviour of the four different sets of material

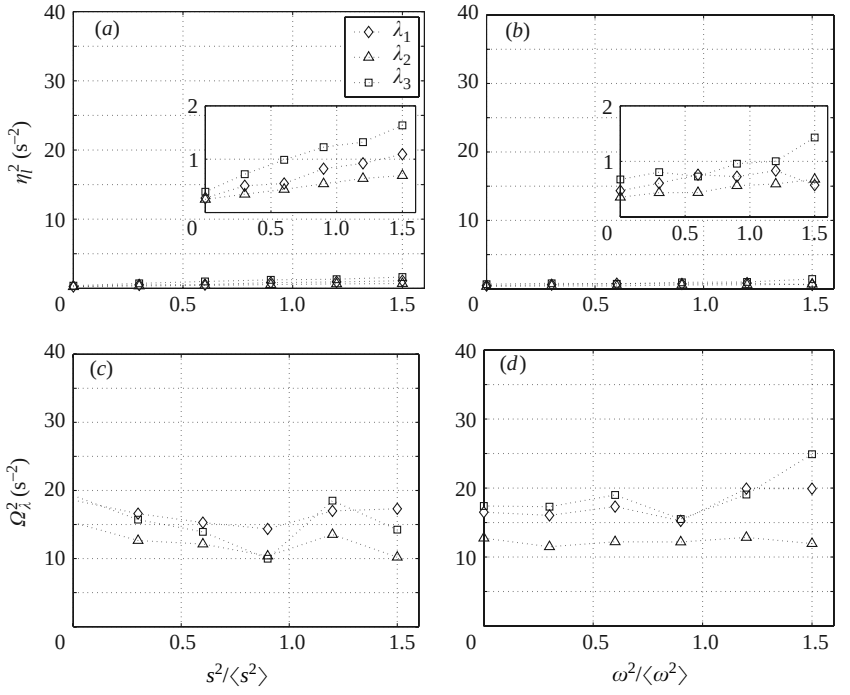

FIGURE 13. Mean contributions of (a, b) the tilting η_l^2 of a material line l_ω initially aligned with vorticity and (c, d) of the rotation of the rate of strain eigenframe Ω_λ^2 in a condition of persistent (l, λ_i) alignment conditioned on strain (left) or enstrophy (right).

lines, as compared to vorticity, is showed in table 6. We immediately note that l tend to maintain their initial orientation more consistently than vorticity. However, material lines were observed to experience switching events, not only towards λ_1, but also away from λ_1. This is almost exclusively caused by the rotation of the eigenframe λ_i, as shown in figures 13 and 14 representing the case of $l \| \omega$. The same behaviour is observed for all the other subsets of l mentioned above. This behaviour is consistent with the non-persistent strain as addressed by Girimaji & Pope (1990). We emphasize that material lines do not significantly change their orientation as often as vorticity does. The contribution of Ω_λ^2 is clearly dominating over η_l^2 for maintaining/switching any (l, λ_i) alignments, while, in the case of the (ω, λ_i) alignments, the influence of Ω_λ^2 is of comparable order of magnitude as Ω_ω^2. This explains also why l tend to maintain their initial orientation more consistently than vorticity, because only λ_i is active, and not both λ_i and ω. The comparative analysis of l and ω behaviour shows that the differences are intrinsically related to the fact that the eigenvectors λ_i of s_{ij} and vorticity are not only coupled, but also particularly non-persistent in their direction, as suggested by Girimaji & Pope (1990), while l is not only passive, but also reluctant to be tilted.

6. Conclusion

The Lagrangian evolution of the stretching of vorticity and the stretching of material lines has been investigated experimentally in a homogeneous turbulent flow in order to shed more light on the different behaviour of vorticity, which is dynamically an active quantity, and material elements, which are passive quantities. The first result is

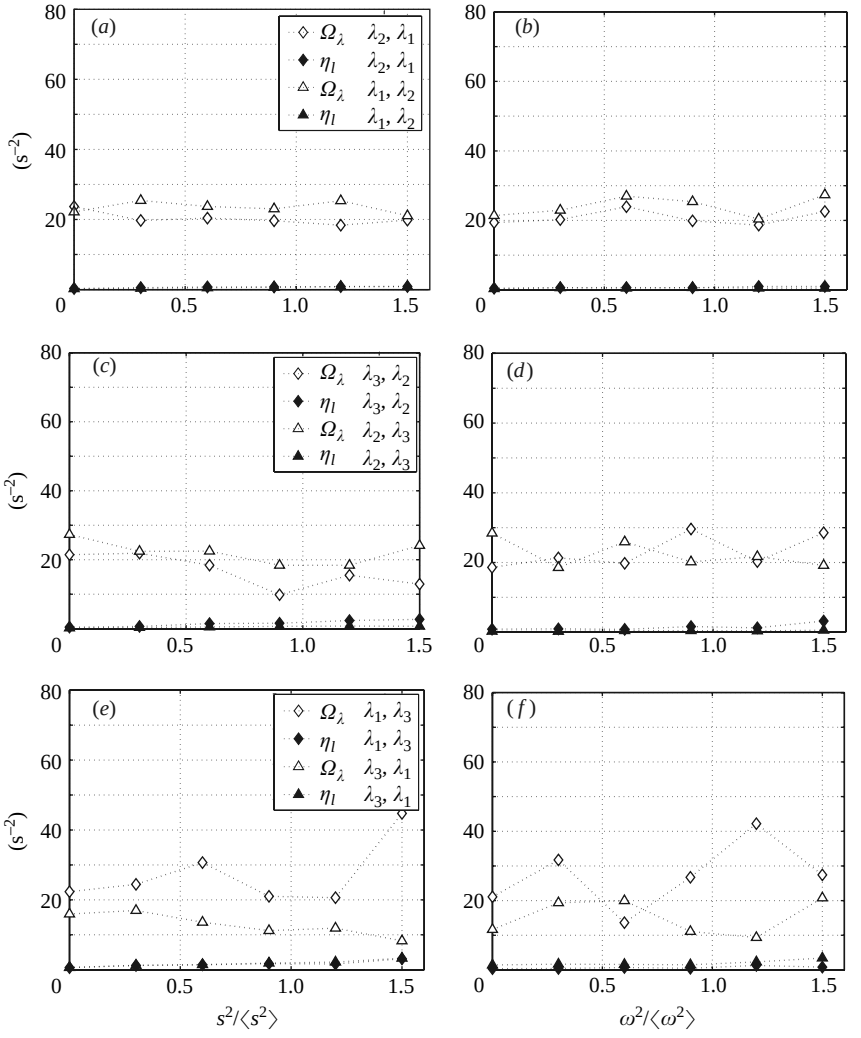

FIGURE 14. Mean contributions of the tilting η_l^2 of the material line l_ω and of the rotation of the rate of the strain eigenframe Ω_λ^2 during the switches (l_ω, λ_i)–(l_ω, λ_j) alignments conditioned on strain (left) or enstrophy (right).

	λ_1	λ_2	λ_3	$\lambda_1\lambda_2$	$\lambda_2\lambda_1$	$\lambda_3\lambda_2$	$\lambda_2\lambda_3$	$\lambda_3\lambda_1$	$\lambda_1\lambda_3$
ω	15	28	6	13	15	6	7	5	3
$l//\omega$	20	30	6	11	15	4	5	4	2

TABLE 7. Overall percentage distribution of the time in which ω is persistently staying on λ_i or switching from λ_i to λ_j and correspondent percentage for l_ω.

that the initial orientation of vorticity/material lines with respect to the eigenframe of the rate of strain tensor λ_i is not a sufficient reason to explain why $\langle \omega_i \omega_j s_{ij}/\omega^2 \rangle < \langle l_i l_j s_{ij}/l^2 \rangle$. Even a material line originally perfectly aligned with vorticity can behave dramatically differently. Theoretical arguments suggested that a key role is played

by both viscosity and the strong interaction between vorticity and strain. Our experimental results confirmed, though indirectly, that viscosity is an absolute crucial quantity. Overall, the inviscid tilting of vorticity is significantly weaker than the effective tilting. This is especially true in the cases of those particular events where the (ω, λ_i) alignment changes. The statistical analysis on the Lagrangian behaviour of the (ω, λ_i) alignments revealed that not only does a self-amplification mechanism of velocity derivatives (Galanti & Tsinober 2000) contribute to the growth of enstrophy, but that also a self-moderating mechanism exists and controls this growth. An analogous mechanism for material element growth control is missing. The main trends observed in this work can be summarized as follows.

(i) In high strain regions, vorticity is definitely reacting back/defending itself to/from persistent stretching, and even more so from persistent compressing, simply by tilting itself with a considerable help from viscosity.

(ii) In high enstrophy regions, the rotation of the eigenframe λ_i, rather than the tilting of vorticity, is responsible for the change of (ω, λ_i) alignments.

(iii) Both the rotation of λ_i and the tilting of vorticity are relatively low when ω is aligned with λ_2.

Vorticity is thus statistically aligned with λ_2 because ω, strain and the viscous term $\nu\omega_i\nabla^2\omega_i$ act towards either maintaining or achieving this alignment.

On the other hand, material lines are substantially stretched along λ_1 and, owing to the non-persistent orientation of the strain eigenframe, they are not only stretched, but also tilted towards λ_1. However, the latter process is much slower compared to the tilting of vorticity because vorticity, assisted by viscosity, is actively and continuously changing its direction as described above, while material lines are very reluctant to change their orientation. In fact, they are observed to tilt mainly because they are significantly stretched along λ_1, that is, changing its direction continuously. The different stretching rates ($\langle\omega_i\omega_j s_{ij}/\omega^2\rangle < \langle l_i l_j s_{ij}/l^2\rangle$) are thus the result of a sum of different behaviours of material lines and vorticity that manifest themselves in the predominant statistical alignment of ω, λ_2 and l, λ_1. Among these differences we emphasize the importance of two physical mechanisms, namely the viscosity-assisted self-moderated growth of vorticity and, on the other hand, the reluctance of material elements to be tilted by the vorticity field versus their tendency to be stretched along a non-persistent λ_1-direction.

These results were obtained for a relatively low Re_λ. However, it seems that, at least qualitatively, they should be valid for large Reynolds number as well. There are at least two indications for this. The first is that the alignment between l and λ_1 is independent of the magnitude of Re_λ. The second is that the ω, λ_2 alignment was observed experimentally at Re_λ as high as 10^4 (Kholmyansky, Tsinober & Yorish 2001). Further justification of our results for larger Reynolds numbers is beyond reach (so far) owing to both experimental and computational limitation.

We gratefully acknowledge funding by the ETH research commission under grant TH 15/04-2.

REFERENCES

Andreotti, B. 1997 Alignment of vorticity and scalar gradient with strain rate in simulated Navier–Stokes turbulence. *Phys. Fluids* **9**, 735–742.

Ashurst, W. T., Kerstein, A. R., Kerr, R. A. & Gibson, C. H. 1987 Alignment of vorticity and scalar gradient with strain rate in simulated Navier–Stokes turbulence. *Phys. Fluids* **30**, 2343–2353.

Brachet, M. E. 1992 Numerical evidence of smooth self-similar dynamics and possibility of subsequent collapse for three-dimensional ideal flows. *Phys. Fluids* A **4**, 2845–2854.

Dresselhaus, E. & Tabor, M. 1991 The kinematics of stretching and alignment of material elements in general flow fields. *J. Fluid Mech.* **236**, 415–444.

Drummond, I. T. & Münch, W. 1990 Turbulent stretching of line and surface elements. *J. Fluid Mech.* **215**, 45–59.

Galanti, B. & Tsinober, A. 2000 Self-amplification of the field of velocity derivatives in quasi-isotropic turbulence. *Phys. Fluids* **12**, 3097–3099.

Girimaji, S. S. & Pope, S. B. 1990 Material-element deformation in isotropic turbulence. *J. Fluid Mech.* **220**, 427–458.

Huang, M. J. 1996 Correlations of vorticity and material line elements with strain in decaying turbulence. *Phys. Fluids* **8**, 2203–2214.

Kholmyansky, M., Tsinober, A. & Yorish, S. 2001 Velocity derivatives in the atmospheric surface layer at $Re_\lambda = 10^4$. *Phys. Fluids* **13**, 311–314.

Kida, S. & Goto, S. 2002 Line statistics: stretching rate of passive lines in turbulence. *Phys. Fluids* **14**, 352–360.

Lüthi, B., Tsinober, A. & Kinzelbach, W. 2005 Lagrangian measurement of vorticity dynamics in turbulent flows. *J. Fluid Mech.* **528**, 87–118.

Majda, A. J. 1991 Vorticity, turbulence and acoustics in fluid flow. *SIAM Rev.* **33**, 349–388.

Nomura, K. K. & Post, G. K. 1998 The structure and dynamics of vorticity and rate of strain in incompressible homogeneous turbulence. *J. Fluid Mech.* **377**, 65–97.

Ohkitani, K. 2002 Numerical study of comparison of vorticity and passive vectors in turbulence and inviscid flows. *Phys. Rev.* E **65**, 046304, 1–12.

Su, L. K. & Dahn, W. J. A. 1996 Scalar imaging velocimetry measurement of the velocity gradient tensor field in turbulent flows. II Experimental result. *Phys. Fluids* **8**, 1883–1906.

Tsinober, A. 2001 *An Informal Introduction to Turbulence*. Kluwer.

Tsinober, A. & Galanti, B. 2003 Exploratory numerical experiments on the differences between genuine and 'passive' turbulence. *Phys. Fluids* **15**, 3514–3531.

Willneff, J. & Gruen, A. 2002 A new spatio-temporal matching algorithm for 3D-particle tracking velocimetry. *Proc. 9th Intl Sym. on Transport Phenomena and Dynamics of Rotating Machinery, Honolulu, Hawaii.*